Molecular Simulation, 2013
http://dx.doi.org/10.1080/08927022.2013.811723

Molecular dynamics simulation of formation and growth of CdS nanoparticles

Farzaneh Shayeganfar[a], Zahra Eskandari[a], M. Reza Rahimi Tabar[a,b] and Muhammad Sahimi[c]*

[a]*Department of Physics, Sharif University of Technology, Tehran 11365-9161, Iran;* [b]*Institute of Physics, Carl-von-Ossietzky University, D-26111 Oldenburg, Germany;* [c]*Mork Family Department of Chemical Engineering & Materials Science, University of Southern California, Los Angeles, CA 90089-1211, USA*

(*Received 28 October 2012; final version received 1 June 2013*)

Monodispersed semiconducting nanoparticles are usually synthesised in a liquid medium using injection of an appropriate solution. A key factor in attaining a narrow particle size distribution (PSD) is the temporal separation of the nucleation and growth stages, where the former takes place during the injection. Faster injection produces a larger number of nuclei and a narrower PSD. The injection speed is expected to affect the diffusion of the ions in the solution and to create uniformly high supersaturation for a short period of time. In this paper, we study the growth of CdS nanoparticles during the injection by molecular dynamics simulation. A solution of Cd ions is injected into the simulation cell that contains sulphure ions; the variation of the PSD and its mean and variance are studied as functions of the injection velocity. Higher injection velocities produce narrower PSDs and smaller particles, hence providing a precise method for controlling both.

Keywords: CdS nanoparticle; molecular simulation; semiconducting particles

1. Introduction

Semiconducting nanoparticles exhibit novel quantum size effects that make them attractive for applications such as biological labelling,[1,2] electroluminescent devices,[3,4] optical amplifier media [5] and solar cells.[6,7] For many applications monodispersity of the particles' size is a requirement, as discrete energy levels can only be distinguished in a single-sized collection of particles. In their early work, Lamer and Dinegar [8] demonstrated that the growth of monodispersed colloidal particles is possible through controlling their supersaturation in such a way that the growth stage is temporarily separated from the nucleation stage. Various monodispersed colloids of the II–VI and III–V semiconducting nanoparticles have been synthesised using this strategy.[9–11]

In this paper, we study the formation of CdS nanoparticles, which are semiconducting materials with a broad range of applications. An important example of such semiconducting materials, which is also closely related to our work, is CdSe nanoparticles.[12,13] Under the bulk conditions, CdSe and CdS, both direct-gap materials, exhibit several similarities. They both adopt the hexagonal Wurtzite structure, which leads to similar electronic band structure and properties. Thus, it is instructive to consider how CdSe particles are formed in experiments. In a typical experiment to produce monodispersed CdSe nanoparticles, one of the reactants is rapidly injected into a vessel that contains the other reactants and is usually at a high temperature. Nucleation takes place shortly after the injection due to the very high supersaturation of the monomers. Over a limited time period after the nucleation, the supersaturation level remains high and the system is far from thermodynamic equilibrium. Under such conditions, the initial nanoparticles grow at the expense of the monomers in such a way that a narrower particle size distribution (PSD) is obtained.[14] Further growth under low-supersaturation condition results in Ostwald ripening and a slow broadening of the PSD. It is, therefore, important to maintain the high-supersaturation condition during the growth of the nanoparticles, either by stopping the growth before complete monomer depletion, or by adding new monomers into the reaction vessel.[15]

An experimentally established fact about the synthesis of semiconducting nanoparticles by the injection method is that, the quality of the nanoparticles, i.e. the narrowness of their PSD, depends on the injection speed. This has sometimes made the results less reproducible, as the injection speed is usually not measured and controlled. In an ideal case, the injection takes place in a very short time and with a very high velocity, which results in a uniformly high-supersaturated solution by rapid diffusion of the injected reactants throughout the reaction solution and the formation of a large number of initial nuclei. It is, therefore, desired to produce the largest number of nuclei in the nucleation stage. At the other extreme, in slow injection and subsequent slow diffusion of the injected reactants, larger nuclei with a broader PSD are formed, which result in a smaller number of the nuclei, because supersaturation at the injection point is distinctly different from that in areas of the vessel that are far from it. The supersaturation level also differs during the injection time.

*Corresponding author. Email: moe@usc.edu

In a previous study,[16] hereafter referred to as Part I, we reported the results of an experimental study of the formation of CdS nanoparticles. Fabrication of CdSe nanocrystals in nanolitre droplets was reported previously by Chan et al. [17], who utilised a flow-focusing nanojet structure. The method that we used for producing the CdS nanoparticles was based on the aforementioned injection technique. In this study, we carry out molecular dynamics (MD) simulation of the same process, in order to obtain better understanding of the effect of the injection speed on the initial stage of the growth of the CdS nanoparticles. As described earlier, in an efficient system for monodisperesed growth, supersaturation should be maintained at a high level after injecting the reactants, in order to obtain a narrower PSD. Smaller nanoparticles are formed during the injection, which implies a larger number of the nuclei. Therefore, we seek through MD simulations the conditions that result in smaller nanoparticles during the injection period and shortly thereafter.

The rest of this study is organised as follows. In the next section, we briefly describe the reactive system that results in the formation of the CdS nanoparticles. Section 3 describes the molecular models for the various ions, as well as the force field used in the MD simulations. The procedure for carrying out the MD simulations is described in Section 4. The results are presented and discussed in Section 5, and Section 6 summarises the paper.

2. The reactive system

The reaction that produces the CdS nanoparticles in our experimental system [16] is one between $Cd(NO_3)_2$ and Na_2S:

$$Cd(NO_3)_2 + Na_2S \rightarrow CdS + 2Na(NO)_3.$$

The CdS nanoparticles are formed quickly.[16] The Cd $(NO_3)_2$ solution is injected into the Na_2S solution with velocity v_0. Therefore, by adjusting v_0 we create high-speed mixing in the solution. A high-speed injection prevents the small particles from agglomeration, hence providing a precise method for controlling their size. This was also used in our experimental study.[16]

3. Molecular models and the interaction potentials

In order to gain a molecular-level understanding of the physical phenomena that produce the CdS nanoparticles in the experiments, we utilised MD simulation [18] using the LAMMPS package [http://lammps.sandia.gov/other.html]. The MD simulation also enables us to compute the quantities that are not easily accessible in experimental studies of this type, such as the PSD. We emphasise that the MD simulations are utilised mostly for gaining a molecular-level understanding of the phenomena involved in the fabrication of the nanoparticles, rather than quantitative estimates of the properties.

MD simulations of nanoscale materials [19] and, in particular, nucleation and growth of nanoparticles [20] have been carried out in the past, although many of them were for nanoparticles grown in a vapour phase, rather than in a liquid environment that is of interest to us in this paper. They include MD simulations for gold,[21] C_{60},[22] NaCl,[23] strontium chloride [24] and silver [25] nanoparticles. To our knowledge, despite its significance, no MD study of the formation of CdS nanoparticles in a solution has ever been carried out.

A cell of size 30 nm × 30 nm × 30 nm was used in the MD simulations, so chosen to achieve the correct solution density that had been used in our experiments.[16] The water molecules were represented by the TIP3P model [26] and its parameters (see Table 1). The size and energy parameters of pairs of atoms were computed using the Lorentz–Berthelot mixing rule, $\sigma_{ij} = 1/2\,(\sigma_i + \sigma_j)$, and $\varepsilon_{ij} = \sqrt{\varepsilon_i \varepsilon_j}$. The same procedure is used for calculating the effective parameters for the $(CdS)_n$ aggregates and a single CdS molecules (although, admittedly, this is only a rough representation of the atomistic structure of such molecules). As usual, the molecules moved according to the equations of motion that represent the balance between the gravitational effect (falling or buoyancy) and the viscous drag. The number of water molecules was 900, that of Cd^{++} was 60, while there were typically about 300 S^- ions in the solution. Thus, for every S^- ion we used three water molecules, and for every Cd^{++} ions we had five S^- ions, which is the same as in Part I.

The non-bonded interactions between the Cd^{++} and S^- are of Coulomb and van der Waals type, with the latter interaction represented by a Lennard-Jones (L-J) 6–12 potential:

$$E_{\mathrm{nb}} = \sum_i \sum_j \frac{k_c\, q_i\, q_j}{r_{ij}} + \frac{A}{r_{ij}^{12}} - \frac{B}{r_{ij}^{6}}, \qquad (1)$$

Table 1. Numerical values of the MD simulation parameters. The parameters for water are those of the TIP3P model.

Group or ion	σ (Å)	ε (kcal/mol)	Partial charge
OO	3.1507	0.1521	
HH	0.4000	0.0460	
OH	1.7753	0.0836	
S^-	3.55	0.25	−2.00
Cd^{++}	2.70	0.0059	+2.00
O (H_2O)			−0.834
H (H_2O)			+0.417
Na^+	2.35	0.1301	+1.00
N (NO_3^-)	3.06	0.0257	+0.95
O (NO_3^-)	2.774	0.18	−0.65

Note: The parameters for NO_3^- were taken from Ribeiro [43].

where q_i is the partial charge of molecule or ion i, and k_c, A and B are constant. All the L-J parameters and the partial charges are given in Table 1 (including those of Na^+ and NO_3^-), where the water parameters represent those for the TIP3P model,[26,27] and those for Cd^{++} and S^- were taken from Zhai et al. [28] and de Araujo et al. [29]. The equilibrium length of the OH bond was taken to be 0.9572 Å, the HOH angle was 104.52°, the SHAKE algorithm [30–32] was used to keep the length of the OH bond and the HOH angle fixed, while $A = 582{,}000\,\text{kcal}\,\text{Å}^{12}/\text{mol}$ and $B = 595.00\,\text{kcal}\,\text{Å}^6/\text{mol}$. The interactions between the CdS particles and $(CdS)_n$ clusters were also represented by the L-J potential, where n is the number of CdS molecules in the cluster.

As pointed out by Yasuoka and Matsumoto [33], the definition of a cluster in the type of nucleation and growth simulations that we carry out is somewhat arbitrary. Two molecules may be considered as clustered (connected), if the distance r_0 between their centres of mass is less than a critical value, say $r_0 = 1.5\sigma$, where σ is the L-J size parameter of the smallest molecule or ion. Alternative definitions of σ based on, for example, the minimum of the radial distribution function of the L-J liquids near the triple point is also possible.[34] But, this is still somewhat arbitrary, because it relies on *instantaneous* configurations. Thus, a better definition, used in this work, is that the distance r_0 must satisfy the aforementioned criterion, *and* it does so for three time steps of the simulations or longer.

A main advantage of using the periodic boundary conditions is that they allow accurate computation of long-range electrostatic interactions through the particle-mesh Ewald (PME) summation method.[35] In general, the electrostatic charges are derived from the polarity of the water molecules, the ions in the solution and the mobility of the charged molecules. The interactions between the charge centres are important because they are the main long-range forces in the MD simulations. In order to compute efficiently the effect of the charges in the system, the PME algorithm was used to compute the Coulombic interactions. As each atom interacts with all the other atoms in the system, the time required to compute the long-range interaction potentials scales with the square of the number N of the atoms, if the PME method is not used.[35–37] The PME algorithm, an improved version of the Ewald summation method, makes it possible to compute the interactions more efficiently and, thus, allows the MD simulations with a large number of atoms to be carried out.[38] It scales as $O(N \log N)$ and, thus, is very efficient. Thus, we used periodic boundary conditions in the planes perpendicular to the direction of injection (see Figure 1), when we generated the molecular model of water five solution, in order to properly account for the effect of long-range electrostatic interactions.

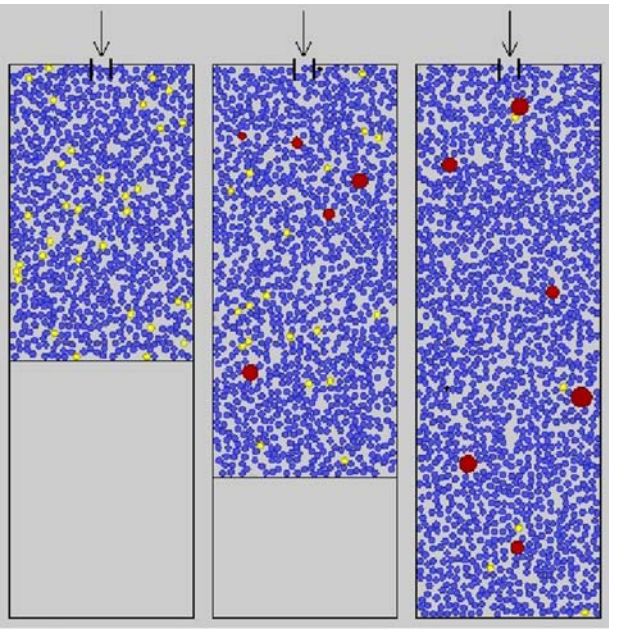

Figure 1. (Colour online) Snapshots of the simulation cell. H_2O molecules (blue), S^- (yellow), Cd^{++} (black) and $(CdS)_n$ clusters (red) are shown. In the first step (left), only water molecules, S^- and Cd^{++} are in the system. In the second step (centre), Cd^{++} plus water molecules enter the system regularly. Then (right), there is the possibility of forming the CdS nanoparticles and the $(CdS)_n$ clusters. The region for injecting Cd^{++} ions is shown at top of the figures.

4. MD simulation

Figure 1 shows the front view of the system. The Cd ions were injected into the system at the top. The procedure for the MD simulations was as follows. First, the water molecules were generated and the S^- ions were inserted into the simulation cell, as shown in Figure 1. The initial configuration was then relaxed to ensure that it was in equilibrium. This was achieved by MD simulations, first in the *NVT* ensemble for 5000 time steps, followed by additional simulations in the *NPT* ensemble for another 5000 time steps. The time step was 0.1 ps. If an ion collided with the walls, the direction of its velocity was reversed in the opposite direction. $Cd(NO_3)_2$ molecules were then injected into the simulation cell that contained the Na_2S solution. Five injection velocities, $v_0 = 100$, 200, 300, 400 and 500 cm/s were used, so selected to make this simulation parameter to be the same as the injection speeds used in the experiments, reported in Part I. The time interval τ between injection of two $Cd(NO_3)_2$ may be estimated, given the injection velocity v_0 and the diameter of the entrance to the system. If such times are assumed to be independent of each other, then their distribution $f(\tau)$ may be assumed to be exponential,

$$f(\tau) = t_0^{-1} \exp(-\tau/t_0). \tag{2}$$

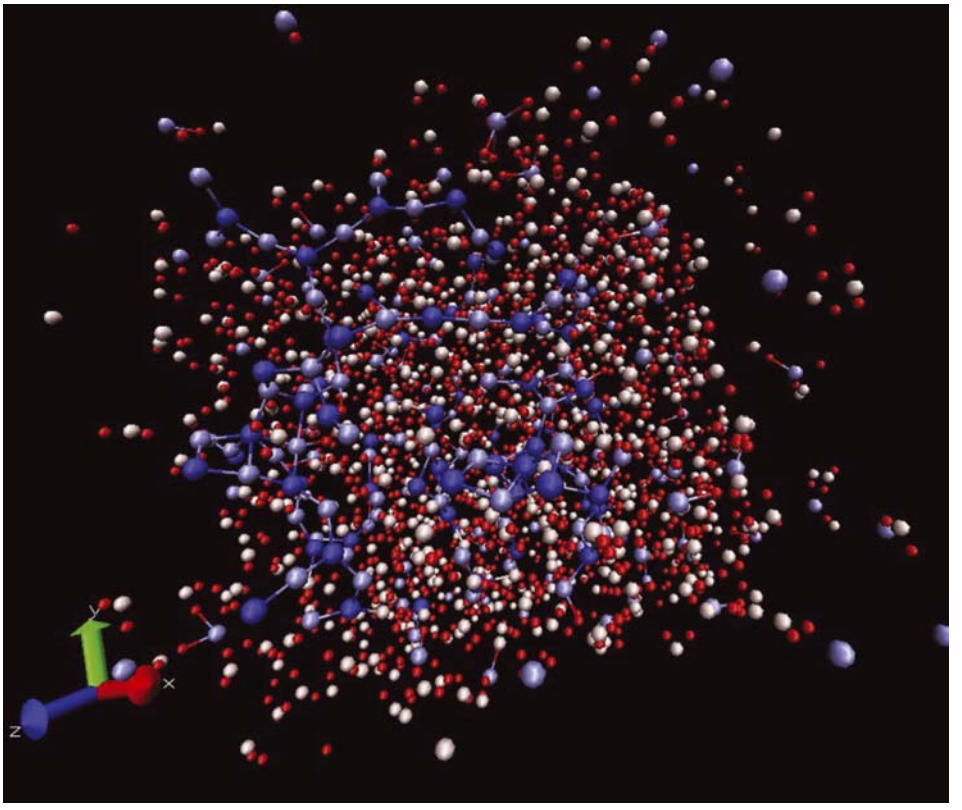

Figure 2. (Colour online) A snapshot of the simulation cell. H_2O molecules are shown with white (O) and red (H) circles, S^- ions with dark blue circles, Cd^{++} ions with light circles and $(CdS)_n$ clusters with bonds.

Thus, after generating the water molecules, inserting the S^- ions and relaxing the system, the injection of $Cd(NO_3)_2$ commenced and continued at time intervals selected from the distribution (2), until they were all in the system. The constant t_0 was taken to be 1 ns. Due to the use of a random time interval between injection of the Cd^{++} ions, their number was not fixed. Each time a Cd^{++} ion collided with an S^-, they were replaced by a CdS molecule. This is permissible because CdS is insoluble in water and its ionisation energy at room temperature (rt) is much larger than k_BT, with k_B being the Boltzmann's constant and T the temperature. Similarly, upon collision of a CdS molecule with a $(CdS)_n$ cluster, the cluster was grown by one CdS molecule, $n \rightarrow n + 1$. The simulations were carried out at rt, 300 K. Temperature was held constant using the Berendsen thermostat.[39]

The Verlet velocity algorithm was used for integrating the equations of motion. To begin integrating the equations, the injection velocity was added to the thermal velocities of the Cd^{++} ions and the water molecules. This step was continued until the total number of the Cd^{++} ions (six) that were to be added to the initial solution containing S^- and the water molecules were all used up. As a result of injecting the Cd^{++} ions, the CdS nanoparticles nucleated and $(CdS)_n$ clusters began to form. Formation of the CdS nanoparticles and $(CdS)_n$ clusters continued until there was no variations in the *type* of the particles, implying that there were no longer any free Cd^{++} and S^- ions in the solution and, in addition, there was no single (not clustered) CdS nanoparticle in the solution. Care was taken to ensure that injection of the ions into the system did not lead to the violation of momentum balance within the simulation cell.

To compute efficiently the L-J and Coulombic interactions, an additional switching function $S(r)$ was used,[40] that ramps the energy and forces smoothly to zero between an inner and an outer cut-off radii. The inner and outer cut-off radii were set, respectively, to be 8 and 10 Å, after some preliminary simulations, indicating that a larger cut-off would not change the qualitative aspects of the results. Note that the outer cut-off is about three times larger than the radius of the bigger ion, S^-, and that our main interest in this paper is obtaining qualitative insight into the phenomena that take place.

5. Results and discussion

In what follows, we present and discuss the results. The estimated errors for all the quantitative results that are

described below are about ±15% of the data that are shown in the figures.

5.1 Cluster formation

Figure 2 shows some snapshots of the system. Figure 3 shows two other snapshots in which the water molecules are not displayed, in order to show the distribution of the $(CdS)_n$ clusters more clearly. The snapshots shown are for injection velocities of $v_0 = 500$ and 100 cm/s of Cd $(NO_3)_2$, and represent the state of the system after 15 ns. It is clear that a higher injection velocity produces smaller $(CdS)_n$ cluster with low values of n. This implies that the CdS nanoparticles are created gradually, but grow over longer times to larger particle clusters. Hence, longer MD runs are required for low values of the injection velocity v_0.

The MD simulations also indicate that, for a large enough injection velocity v_0, one has two regions in the system. One, near the injection point, is populated mostly by the Cd^{++} ions, whereas the second region farther away from the injection point contains mostly S^{-}. Clearly, the two regions influence the formation of the nanoparticles, and partly explain why large particles are not formed for large v_0.

5.2 Particle size distribution

To compute the PSD, we carried out 20 independent MD simulation runs for every injection velocity. This was necessitated by the fact that the time τ between two consecutive injections was selected at random according to Equation (2). Every MD run produced some of the $(CdS)_n$ clusters with various cluster numbers n. The PSD was then computed by counting the number of the CdS nanoparticles as a function of n in all the runs, and converting the results to corresponding sizes of the nanoparticles, in order to compute the PSD. As every run also produces various cluster sizes, we also computed the average diameter $\langle d \rangle$, with the average taken over all the runs and the clusters.

Figure 4 shows the PSD for the highest and lowest injection velocities that we simulated, while Figure 5 shows the distribution of the cluster number n for the same injection velocities, where n is the number of the CdS particles that stick together and form the clusters. They were both computed after 15 ns of simulations. As Figure 4 indicates, not only is the MD-computed PSD at high v_0 narrower than the corresponding one at low v_0, but also it

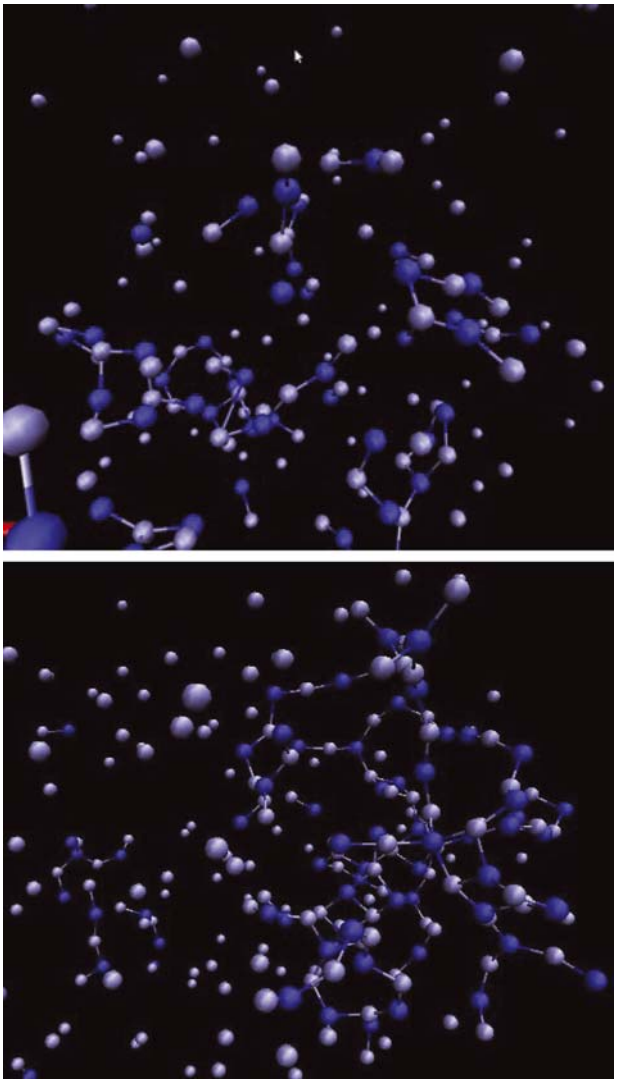

Figure 3. The distribution of the $(CdS)_n$ clusters for two injection velocities v_0. Top: $v_0 = 500$ cm/s and bottom: $v_0 = 100$ cm/s. For better clarity the water molecules are not shown.

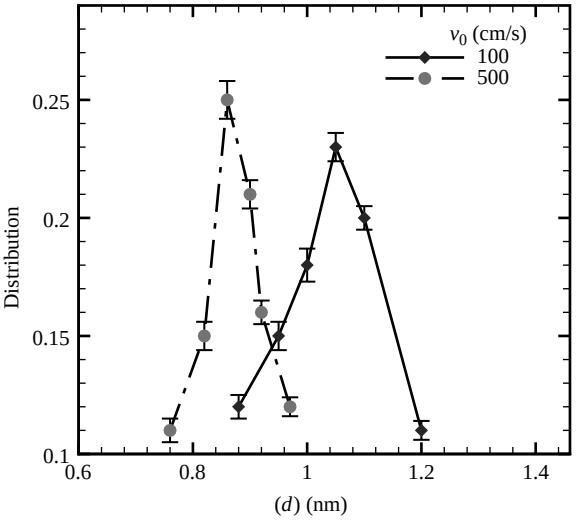

Figure 4. The computed PSD, where $\langle d \rangle$ is the mean size of the $(CdS)_n$ particles.

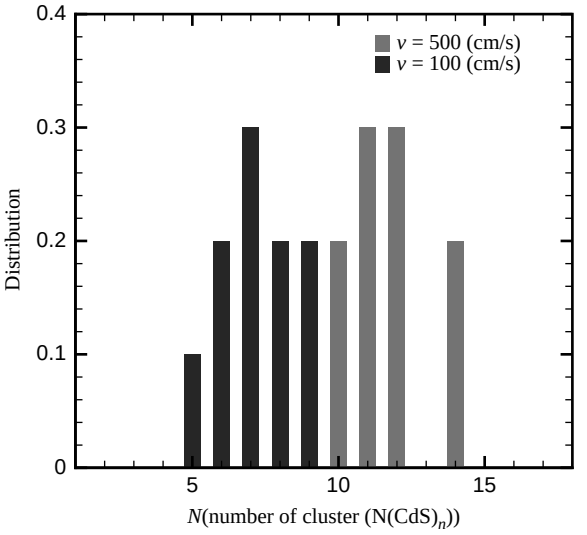

Figure 5. The distributions of the size n of the $(CdS)_n$ clusters for two injection velocities v_0.

has a larger maximum, hence indicating that a larger fraction of the nanoparticles has smaller sizes.

Figure 6 shows the dependence of the average diameter $\langle d \rangle$ of the particles on the injection velocity v_0. Higher velocities cause better mixing and, hence, produce lower average particle sizes. To reconfirm the trends shown in Figure 6, we also computed the variance of the PSD and its dependence on the injection velocity v_0. The results are shown in Figure 7. Once again, higher injection velocities produce narrower PSD and, therefore, smaller variances. Both the average and variance of the particles' sizes depend relatively weakly on the injection velocity, in agreement with the experimental data.[16]

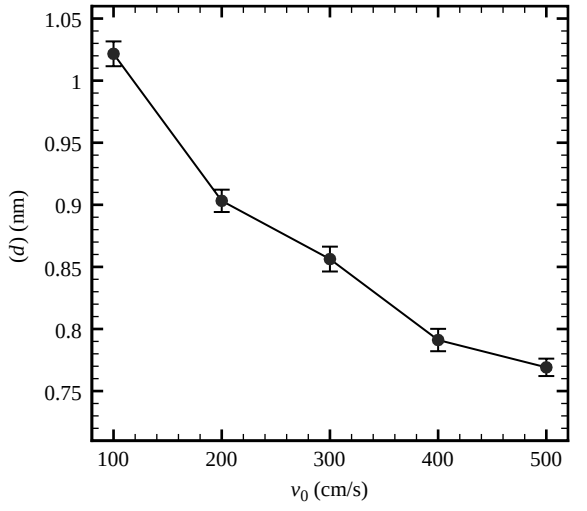

Figure 6. The dependence on the injection velocity v_0 of the average diameter $\langle d \rangle$ of the CdS nanoparticles.

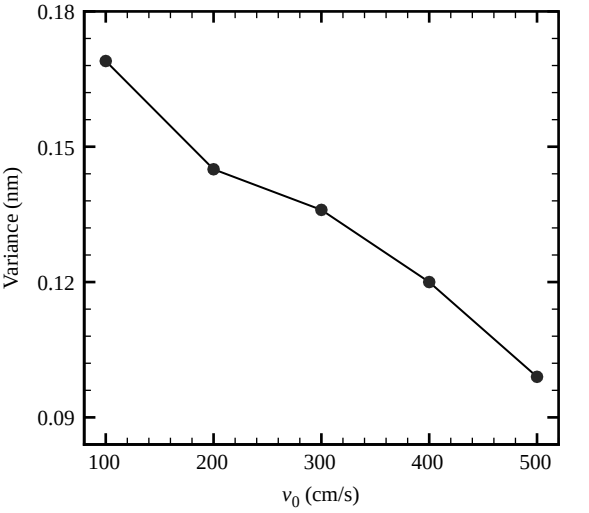

Figure 7. The dependence on the injection velocity v_0 of the variance of the PSD of the CdS nanoparticles.

The relatively weak dependence of the average and variance of the particles' sizes on the injection velocity deserve a more thorough discussion, as it might appear to contradict what is already known about homogeneous nucleation. For example, in an extensive study by MD simulations, Yasuoka and Matsumoto [33] investigated homogeneous nucleation in the vapour phase. They began their simulations with an almost uniform spatial distribution of the particles (see their Figure 3) and studied the evolution of the cluster size distribution. At early stages many small clusters were formed, but were then broken by molecular collisions. After some time some of the clusters that were larger than a critical size survived. The authors referred to this step as Stage I of the nucleation process. At longer times the cluster formation entered Stage II in which the rate of the growth was essentially constant.

The system that we study is not, however, homogeneous at the initial stage. Only the S^- ions are almost uniformly distributed in the system. The Cd^{++} ions are injected into the solution through the small orifice at the top of the system. High-speed injection generates large interfacial surface that permits slow molecular mixing to proceed efficiently. The nanoparticles grow by two mechanisms [16]: picking up the non-nucleated product molecules and coagulating the small nanoparticles. The initial growth of the nanoparticles is primarily through the former mechanism, because the probability of collision between the two reactants is high. After all the reactants have been consumed to form the particles, coagulation is the only mechanism that allows them to grow further. Therefore, if the surface that separates the two ions or mixing layers is large enough (for high-velocity injection), then CdS nucleation will take place on a surface A far from

the two ions, increasing the number of the CdS nucleation. As a result of the small particles being created, if the surface A is small (smaller injection speeds), the distance between the CdS nucleation will be very small and will cause the coagulation of the nanoparticles. This is clearly shown in Figures 4–7.

5.3 Comparison with experimental data

It might be instructive to compare the results obtained with the MD simulations with the experimental data.[16] The experimental data were, however, measured in terms of a Reynolds number (*Re*) of the injection defined by, $Re = v_0 D/\mu$, where D and μ are, respectively, the diameter of the nanojet injection orifice and the average viscosity of the solution. Previously,[16] we reported the data for a range of *Re*. High *Re* injections cannot, however, be simulated by the MD simulations. Our experiments indicated that the transition to turbulence in the system begins at a *Re* of about 600. Moreover, whereas the experiments were carried out in a macroscopic system, the simulations were carried out in a nanosize cell. Therefore, the two sets of the results may not be directly comparable.

The viscosity of a solution in a nanoscale system is different from that of the bulk solution.[41,42] But, regardless of its value relative to the bulk, the solution viscosity does not vary greatly and, moreover, D, the diameter of the nanojet, is also constant. Thus, a qualitative comparison between the MD simulation results and the experimental data might be made based on the dependence of the computed quantities on the injection velocity v_0 in the MD simulations on the one hand, and on the *Re* in the experiments,[16] on the other hand. *Surprisingly*, the trends in both sets of data are completely similar.

Figure 8 shows the growth with time of the mean diameter $\langle d \rangle$ of the nanoparticles for the smallest and largest injection velocities used in the MD simulations. For comparison, we show in Figure 9 the measured data for two values of the *Re*, one of which, 2400, was the largest *Re* in the measurement reported in Part I. The qualitative features of the two figures are in excellent agreement. In particular, the MD results indicate that while at *short times* the larger velocity produces larger particles, the trend is reversed at longer times, in qualitative agreement with the experimental data that indicates the same in terms of the *Re*.

Figure 10 shows the growth with the time of the MD-computed mean number of $(CdS)_n$ clusters and its dependence on the injection velocity v_0. For comparison, we show in Figure 11 the dependence of the same quantity, measured experimentally, on the *Re*. Once again, the qualitative features of the two figures are in excellent agreement, including the fact that for larger injection

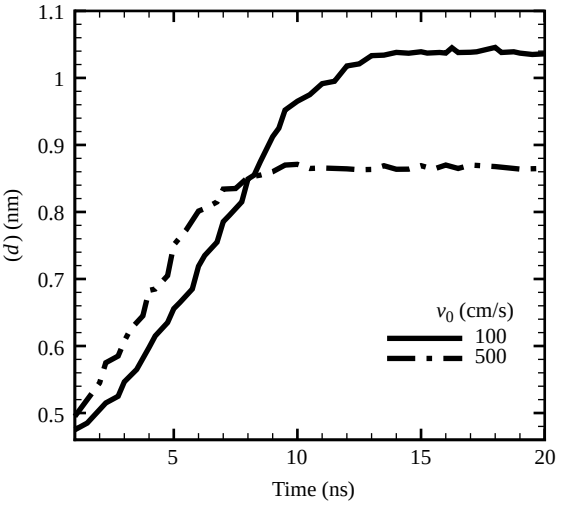

Figure 8. The growth with time of the mean diameter $\langle d \rangle$ and its dependence of the injection velocity v_0, as computed by the MD simulation.

velocity v_0 (injection *Re*), a larger number of (smaller) particles are formed.

Figure 10 can also be used to determine the nucleation rate [33] of the particles. The nucleation rate is typically defined as the number, per unit volume and unit time, of the nuclei larger than a critical size. Thus, if a critical threshold for the size is set, the number of $(CdS)_n$ clusters may be counted and plotted versus time, in a manner similar to Figure 10, but with a particle size threshold imposed. Clearly, if the critical size is large enough, then, although the total number of such nanosize clusters may increase at first, it will eventually decrease and approach a constant for large threshold sizes. Then, the nucleation rate

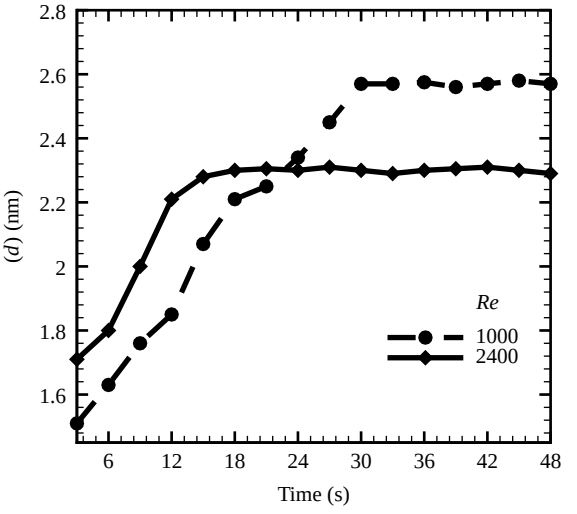

Figure 9. Experimental data for the time growth of the mean diameter $\langle d \rangle$ of the nanoparticles and its dependence on the *Re* of the injection.

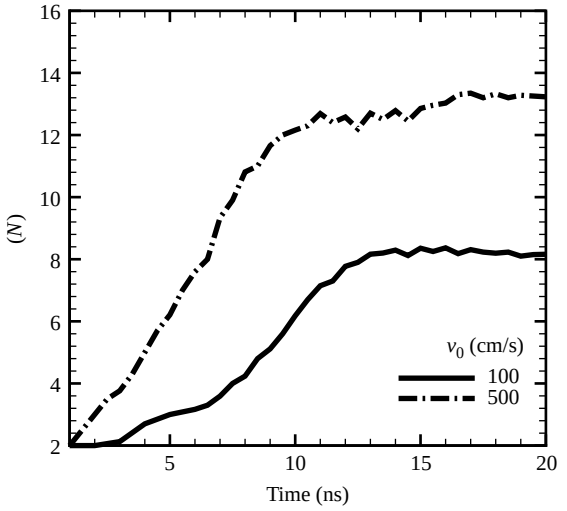

Figure 10. The growth with time of the mean number of clusters and its dependence on the injection velocity v_0, as computed by the MD simulation.

will simply be the slope of such a curve, normalised with the volume of the system.

The qualitative agreement between the MD results and the experimental data indicates the accuracy and power of the former for providing deeper insight into the process of nucleation and growth of nanoparticles by the type of the experimental system described in Part I, and simulated qualitatively in this study.

6. Summary

Extensive MD simulations were carried out in order to study the effect of 10 injection velocity on the growth and size of CdS nanoparticle that are produced by a nanojet method. We demonstrated through the MD simulations that the PSD is narrower at higher injection velocities. High-speed injections create better mixing, decrease coagulation and force the size of the nanoparticles to saturate quickly. Though our MD simulations cannot access the same values of the *Re* at which the experiments were carried out, the trends shown in Figures 8 and 10 are in agreement with the experimental data.

Hence, both the experiments [16] and the MD results presented in this study indicate one and the same conclusion: nanojets provide a precise way of controlling the size of nanoparticles, by adjusting the injection velocity of the fluids.

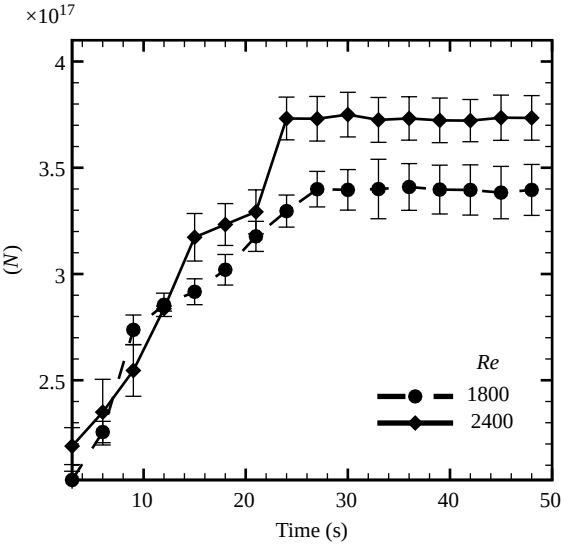

Figure 11. Experimental data for the growth with time of the mean number of clusters and its dependence on the injection *Re*.

Acknowledgement

Work at USC was supported in part by the National Science Foundation.

References

[1] Bruchez MJ, Moronne M, Gin P, Weiss S, Alivisatos AP. *Semiconductor nanocrystals as fluorescent biological labels*. Science. 1998; 281:2013–2016.
[2] Chan WCW, Nie S. *Quantum dot bioconjugates for ultrasensitive nonisotopic detection*. Science. 1998; 281:2016–2018.
[3] Colvin VL, Sclamp MC, Alivisatos AP. *Nanoparticles as catalysts for protein fibrillation*. Nature. 1994; 370:354–357.
[4] Parak WJ, Gerion D, Pellegrino T, Zanchet D, Micheel C, Williams SC, Boudreau R, Gros MAL, Larabell CA, Alivisatos AP. *The use of nanocrystals in biological detection*. Nanotechnology. 2003; 14: R15–R27.
[5] Polman A, Van Veggel FCJM. *Broadband sensitizers for erbium-doped planar optical amplifiers: review*. J Opt Soc Am. 2004; B21:871–892.
[6] Gur I, Fromer NA, Geier ML, Alivisatos AP. *Air-stable all-inorganic nanocrystal solar cells processed from solution*. Science. 2005; 310:462–465.
[7] Nozik AJ. *Multiple exciton generation in semiconductor quantum dots*. Chem Phys Lett. 2008; 457:3–11.
[8] LaMer VK, Dinegar RH. *Theory, production and mechanism of formation of monodispersed hydrosols*. J Am Chem Soc. 1950; 72:4847–4854.
[9] Yu WW, Peng X. *Formation of high-quality CdS and other II–VI semiconductor nanocrystals in noncoordinating solvents: T unable reactivity of monomers*. Angew Chem. 2002; 41:2368–2371.
[10] Murray CB, Norris DJ, Bawendi MG. *Synthesis and characterization of nearly monodisperse CdE (E=sulfur, selenium, tellurium) semiconductor nanocrystallites*. J Am Chem Soc. 1993; 115:8706–8715.
[11] Guzelian AA, Banin U, Kadavanich AV, Peng X, Alivisatos AP. *Colloidal chemical synthesis and characterization of InAs nanocrystal quantum dots*. Appl Phys Lett. 1996; 69:1432–1434.
[12] Murray CB, Kagan CR, Bawendi MG. *Synthesis and characterization of monodisperse nanocrystals and close-packed nanocrystal assemblies*. Annu Rev Mater Sci. 2000; 30:545–610.
[13] Shiang JJ, Kadavanich AV, Grubbs RK, Alivisatos AP. *Symmetry of annealed wurtzite CdSe nanocrystals: assignment to the C_{3v} point group*. J Phys Chem. 1995; 99:17417–17422.
[14] Talapin DV, Rogach AL, Kornowski A, Haase M, Weller H. *Highly luminescent monodisperse CdSe and CdSe/ZnS nanocrystals synthesized in a Hexadecylamine- Trioctylphosphine oxide-Trioctyphosphine mixture*. Nano Lett. 2001; 1:207–211.

[15] Peng X, Wickham J, Alivisatos AP. *Kinetics of II–IV and III–V colloidal semiconductor nanocrystal growth: "focusing" of size distribution*. J Am Chem Soc. 1998; 120:5343–5344.

[16] Shayeganfar F, Javidpour L, Taghavinia N, Rahimi Tabar MR, Sahimi M, Bagheri-Tar F. *Controlled nucleation and growth of CdS nanoparticles by turbulent dispersion*. Phys Rev E. 2010; 81:026304–026308.

[17] Chan EM, Alivisatos AP, Mathies RA. *High-temperature microfluidic synthesis of CdSe nanocrystals in nanoliter droplets*. J Am Chem Soc. 2005; 127:13854–13861.

[18] Allen MP, Tildesley DJ. Computer simulation of liquids. London: Oxford University Press; 1987.

[19] Sahimi M, Tsotsis TT, In: Reich M, Schommers W, editors. Handbook of theoretical and computational nanotechnology. Stevenson Ranch, CA: American Scientific; 2006. Chap. 10.

[20] Suh D, Yasuoka K. *Nanoparticle growth analysis by molecular dynamics: spherical seed*. J Phys Chem B. 2011; 115:10631–10635.

[21] Desgranges C, Delhommelle J. *Phase equilibria of molecular fluids via hybrid Monte Carlo Wang-Landau simulations: applications to benzene and n-alkanes*. J Phys Chem C. 2009; 113:3607–1614.

[22] Ngale KN, Desgranges C, Delhommelle J. *Nucleation and growth of C60 nanoparticles from the supersaturated vapor and from the undercooled liquid: a molecular simulation study.* J Chem Phys. 2009; 131:244515–244521.

[23] Nahtigal IG, Zasetsky AY, Svishchev IM. *Nucleation of NaCl nanoparticles in supercritical water: molecular dynamics simulations*. J Phys Chem B. 2008; 112:7537–7543.

[24] Svishchev IM, Zasestky AY, Nahtigal IG. *Spatial hydration maps and dynamics of naphthalene in ambient and supercritical water.* J Phys Chem C. 2008; 112:20181–20188.

[25] Zeng Q, Jiang X, Yu A, Lu G. *Growth mechanisms of silver nanoparticles: a molecular dynamics study.* Nanotechnology. 2007; 18:035708–035714.

[26] Mark P, Nilsson L. *Structure and dynamics of the TIP3P, SPC, and SPC/E water models at 298K*. J Phys Chem A. 2001; 105:9954–9960.

[27] Graziano G. *Non-intrinsic contribution to the partial molar volume of cavities in water.* Chem Phys Lett. 2006; 429:420–424.

[28] Zhai Q, Li J, Lewis JS, Waldrip KA, Jones K, Holloway PH, Davidson M, Evans N. *Microstructure and electroluminescence of ZnS:Mn doped with KCl.* Thin Solid Films. 2002; 414:105–112.

[29] de Araujo AS, Sonoda MT, Piro OE, Castellano EE. *Development of new Cd2+ and Pb2+ Lennard-Jones parameters for liquid simulations*. J Phys Chem B. 2007; 111:2219–2224.

[30] Ryckaert J-P, Ciccotti G, Berendsen HJC. *Numerical integration of the Cartesian equations of motion of a system with constraints: molecular dynamics of n-alkanes*. J Comput Phys. 1977; 23:327–341.

[31] Yoneya M, Berendsen HJC, Hirasawa K. *A non-iterative matrix method for constraint molecular dynamics simulation*. Mol Simul. 1994; 13:395–405.

[32] Forester TR, Smith W. *SHAKE, rattle, and roll: efficient constraint algorithms for linked rigid bodies*. J Comput Phys. 1998; 19:102–111.

[33] Yasuoka K, Matsumoto M. *Molecular dynamics of homogeneous nucleation in the vapor phase. I. Lennard-Jones fluid*. J Chem Phys. 1998; 109:8451.

[34] Egelstaff PA. An introduction to the liquid state. 2nd ed. Oxford: Oxford University Press; 1992.

[35] Darden T, York D, Pedersen L. *Particle Mesh Ewald-an N.Log(N) method for Ewald sums in large systems*. J Chem Phys. 1993; 98:10089–10092.

[36] Perram JW, Petersen HG, de Leeuw SW. *An algorithm for the simulation of condenced matter that grows as the 3/2 power of the number of particles*. Mol Phys. 1988; 65:875–893.

[37] Mehrabi AR, Sahimi M. *Diffusion of ionic particles in charged disordered media*. Phys Rev Lett. 1999; 82:735–738.

[38] Essmann U, Perera L, Berkowitz ML, Darden T, Lee H, Pedersen LGJ. *A smooth particle mesh Ewald method*. J Chem Phys. 1995; 103:8577–8593.

[39] Berendsen HJC, Postma JPM, Gunsteren WF, DiNola A, Haak JR. *Molecular dynamic with coupling to an external bath*. J Chem Phys. 1984; 81:3684–3691.

[40] Qian X, Schlick T. *Efficient multiple-time-step integrators with distance-based force splitting for particle-mesh-Ewald molecular dynamics simulations*. J Chem Phys. 2001; 116:5971–5984.

[41] Szymański J, Patkowski A, Wilk A, Garstecki P, Holyst R. *Diffusion and viscosity in a crowded environment: from nano- to macroscale*. J Phys Chem B. 2006; 110:25593–25597.

[42] Khademi M, Sahimi M. *Molecular dynamics simulation of pressure-driven water flow in silicon-carbide nanotubes*. J Chem Phys. 2011; 135:204509–204516.

[43] Ribeiro MCC. *Polarization effects in molecular dynamics simulations of glass-formers* $Ca(NO_3)_2{,}nH_2O$, $n = 4$, *6, and 8*. J Chem Phys. 2010; 132:134512–134522.